The Journal of Infectious Diseases

MAJOR ARTICLE

Parvovirus B19V Nonstructural Protein NS1 Induces Double-Stranded Deoxyribonucleic Acid Autoantibodies and End-Organ Damage in Nonautoimmune Mice

Kanoktip Puttaraksa,[1,a] Heidi Pirttinen,[1] Kati Karvonen,[1] Jonna Nykky,[1] Stanley J. Naides,[2] and Leona Gilbert[1]

[1]Department of Biological and Environmental Science and Nanoscience Center, University of Jyvaskyla, Finland; [2]Quest Diagnostics Nichols Institute, Immunology R&D, San Juan Capistrano, California

Background. Viral infection is implicated in development of autoimmunity. Parvovirus B19 (B19V) nonstructural protein, NS1, a helicase, covalently modifies self double-stranded deoxyribonucleic acid (dsDNA) and induces apoptosis. This study tested whether resulting apoptotic bodies (ApoBods) containing virally modified dsDNA could induce autoimmunity in an animal model.

Methods. BALB/c mice were inoculated with (1) pristane-induced, (2) B19V NS1-induced, or (3) staurosporine-induced ApoBods. Serum was tested for dsDNA autoantibodies by *Crithidia luciliae* staining and enzyme-linked immunosorbent assay. Brain, heart, liver, and kidney pathology was examined. Deposition of self-antigens in glomeruli was examined by staining with antibodies to dsDNA, histones H1 and H4, and TATA-binding protein.

Results. The B19V NS1-induced ApoBod inoculation induced dsDNA autoantibodies in a dose-dependent fashion. Histopathological features of immune-mediated organ damage were evident in pristane-induced and NS1-induced ApoBod groups; severity scores were higher in these groups than in staurosporine-treated groups. Tissue damage was dependent on NS1-induced ApoBod dose. Nucleosomal antigens were deposited in target tissue from pristane-induced and NS1-induced ApoBod inoculated groups, but not in the staurosporine-induced ApoBod inoculated group.

Conclusions. This study demonstrated proof of principle in an animal model that virally modified dsDNA in apoptotic bodies could break tolerance to self dsDNA and induce dsDNA autoantibodies and end-organ damage.

Keywords. anti-dsDNA antibody; apoptotic bodies; B19V; glomerulonephritis; SLE.

Viruses are environmental factors that may facilitate the development of autoimmunity and autoimmune disease [1]. Common viruses have been associated with autoimmunity including Epstein-Barr virus (EBV) and parvovirus B19 (B19V) [2–5]; disease associations include systemic lupus erythematosus (SLE), rheumatoid arthritis, myocarditis, fulminant liver failure, and glomerulonephritis (GN) [4, 6]. These viruses utilize the helicase superfamily (SF) SF3 common to small deoxyribonucleic acid (DNA) viruses [5, 7, 8].

In B19V, the multifunctional nonstructural protein 1 (NS1), an SF3 helicase, appears to be a key player in contributing to autoimmunity [9, 10]. Parvovirus B19 NS1 is characterized by a nucleoside triphosphate binding domain, a DNA binding domain, and the ability to provoke host DNA damage leading to apoptosis [6, 9, 11]. We previously demonstrated that expression of B19V NS1 in nonpermissive hepatocytes induced single-strand nicks and NS1-linked bulky adducts in host cell DNA, activated caspase 9, and initiated apoptosis characterized by the formation of cytoplasmic surface blebs that cleave off to form apoptotic bodies (ApoBods) [9, 11, 13]. The ApoBods contain NS1-covalently modified self-DNA and common autoantigens, eg, DNA, Smith (Sm), apolipoprotein H (β2-glycoprotein I), Ku80, and histone H4, and are phagocytized by macrophages [12]. We hypothesized that the high quantity of ApoBods containing altered self-DNA and common autoantigens, including DNA binding proteins, are a critical factor in initiating autoimmunity.

In this study, B19V NS1-induced ApoBods initiated the production of autoantibodies and damage of vital tissues. The appearance of autoantibodies against dsDNA, a marker of SLE [13, 14], was examined as was the impact on autoimmune organ targets. This study highlights a mechanism by which a common virus using a SF3 family helicase can break self-tolerance through reactivity to a viral protein covalently linked to self-DNA.

Received 17 April 2018; editorial decision 3 October 2018; accepted 17 October 2018; published online October 22, 2018.

Presented in part: American College of Rheumatology Annual Scientific Meeting, November 7–11, 2015, San Francisco, CA; 10th International Congress on Autoimmunity, April 6–10, 2016, Leipzig, Germany; American College of Rheumatology Annual Scientific Meeting, November 3–8, 2017, San Diego, CA.

[a]Present affiliation: Mahidol-Oxford Tropical Medicine Research Unit, Faculty of Tropical Medicine, Mahidol University, Bangkok, Thailand.

Correspondence: S. J. Naides, MD, Immunology R&D, Quest Diagnostics Nichols Institute, 33608 Ortega Highway, Immunology 113C, San Juan Capistrano, CA 92675 (stanley.j.naides@questdiagnostics.com).

The Journal of Infectious Diseases® 2019;219:1418–29

DOI: 10.1093/infdis/jiy614

MATERIALS AND METHODS

Animals

BALB/cOlaHsd, 4- to 6-week-old female mice (Harlan Laboratories, Vernay, Netherlands) were maintained at the University of Jyväskylä, under Institutional Review Board no. PH1237A approved by ELLA, the Animal Experiment Board in Finland.

Viral Production

Recombinant B19V NS1 baculoviruses were produced by the Bac-to-Bac baculovirus expression system (Invitrogen) as previously described [12]. Third-generation viruses were tested for transduction efficiency before usage.

Production and Purification of Apoptotic Bodies

Parvovirus B19V NS1 or staurosporine (ST) ApoBods were produced in liver-derived Hep-G2 cells and purified as previously described [12]. Parvovirus B19V NS1 baculoviruses expressed NS1-enhanced green fluorescent protein (eGFP) fusion proteins. The eGFP-expressing ApoBods were not available as controls because eGFP-expressing baculovirus fails to induce ApoBod formation [11]. Purified ApoBods were stored at 4°C before immunization of animals. Apoptotic body concentration was measured using a NanoDrop 1000 spectrophotometer (Thermo Scientific).

Autoimmunity Induction

Mice (6–8 weeks old) were randomly divided into 9 groups (n = 6 mice/group) for different treatments in 2 sets of independent experiments. Mice were immunized twice, on initial treatment day 0 and boosted at week 4, respectively. Negative controls were untreated or treated with 0.5 mL phosphate-buffered saline (PBS), the diluent used for all ApoBod samples. A positive control group was inoculated with 0.5 mL pristane (2,6,10,14-tetramethylpenta-decane; Sigma-Aldrich), a standard inducer of lupus-like disease in mice [15]. Three groups were immunized with B19V NS1-induced ApoBods at 25, 50, or 100 µg per 30 grams body weight, respectively; 3 other groups were inoculated with ST-induced ApoBods at the same concentrations. Mice were treated by subcutaneous injection, except for pristane where peritoneal injection was applied.

Sample Collection

Blood samples were collected at weeks 1, 4, and 8; at week 4, mice received the booster injection after blood collection. At weeks 1 and 4, blood samples were collected from tail veins. At week 8, mice were euthanized, and blood samples drawn by cardiac puncture. Blood samples were clotted at room temperature (RT) for 45 minutes before centrifugation at 850 ×g, and serum was stored at −20°C. Brain, heart, liver, and kidneys were rapidly harvested from the euthanized mice. Organs were dissected by standard procedures [16], and 3- to 5-mm tissue pieces were fixed in 10% formalin in double-distilled water (ddH_2O) at RT for 48 hours.

Crithidia luciliae Immunofluorescence Test Analysis

A commercial *Crithidia luciliae* immunofluorescence test or CLIFT (IFA 1572-1, IIFT *C luciliae* sensitive [anti-dsDNA]; Euroimmun AG, Germany) determined anti-dsDNA antibodies in sera using a fluoresceinated goat antimouse IgG (Euroimmun AG, Luebeck, Germany) as secondary antibody conjugate [17] (see Supplementary Material).

Enzyme-Linked Immunosorbent Assay Analysis

Enzyme-linked immunosorbent assay (ELISA) was used in the detection of anti-dsDNA, as well as anti-eGFP antibodies from mouse sera. Double-stranded DNA isolated from healthy mouse tissues using a commercial DNA isolation kit (DNeasy Blood and Tissue kit; QIAGEN, Germany) was used to assess anti-dsDNA antibody production in mouse sera [18]. In addition, eGFP-coated plates were used in the detection of anti-eGFP antibodies (see Supplementary Material).

Histological Analysis

Tissues were examined by bright-field microscopy (see Supplemental Data).

Nucleosomes Deposit in Kidneys

Paraffin-embedded sections were de-paraffinized and hydrated as described in the Supplement. Endogenous peroxidase was blocked with 3% hydrogen peroxide. Nonspecific binding in samples was blocked with 3% bovine serum albumin (BSA) solution at 4°C overnight. Samples were next washed with 20 dips of Triton solution (0.5% Triton X-100 [Sigma] + 1% BSA + 0.01% sodium azide [NaN_3] in PBS). Mixtures of primary antibodies (25 µL mouse anti-dsDNA (1:500) (MAB1293; EMD Millipore Corporation), rabbit anti-Histone 1 (H1, 1:500) (ab61177; Abcam, Cambridge, UK), rabbit anti-H4 (1:500) (ab52178; Abcam), and rabbit anti-TATA-binding protein ([TBP] 1:200 [ab63766; Abcam] in Triton solution) were placed on each sectioned tissue and incubated at RT for 30 minutes. Samples were washed thrice in Triton buffer for 5 minutes each, then blocked with BSA solution for 30 minutes before secondary antibody mixtures (25 µL) of Alexa Fluor 488 goat antimouse immunoglobulin (Ig)G (H+L) (A11001; Life Technology) and Alexa Fluor 555 goat antirabbit IgG (H+L) (A21428, Life Technology) at a dilution of 1:200 each in Triton solution were placed on each sectioned tissue, and incubated in the dark at RT for 1 hour. Samples were washed thrice with Triton solution for 5 minutes each. To prevent autofluorescence, Sudan black B blocking was used. Before blocking, samples were immersed in ddH_2O for 20 dips. All samples were placed into 0.1% Sudan black B (Merck) in 70% ethanol in the dark at RT for 25 minutes. Samples were washed with 3 changes of ddH_2O for 5 minutes each to remove the remaining Sudan black B solution. Finally, samples were mounted with Prolong Diamond antifade mountant with 4',6-diamidino-2-phenylindole ([DAPI] P36962; Thermo Scientific) to stain the kidney

cell nuclei. Slides were stored at 4°C in the dark. Fluorescent images were obtained using confocal microscopy.

Imaging

Differential interference contrast images were acquired simultaneously with the green fluorescent imaging at the excitation wavelength of 470 nm. Histological severity scores were assessed based on an inflammation and cellular degeneration grading system modified from various established scoring systems (Table 1). Olympus FV10-ASW with a FluoView-1000 confocal microscope (Olympus) was used to assess the fluorescent images of deposited self-antigens in kidney sections at excitation wavelengths of 405 nm for blue fluorescence (DAPI), 488 nm for green fluorescence (Alexa Fluor 488), and 543 nm for red fluorescence (Alexa Fluor 555). The glomerulus was selected as the region of interest to identify the nucleosomal antigen deposition, including dsDNA and H1/H4/TBP, in the structures of the kidneys, and prominently the glomerular basement membranes (GBMs). The intensity of labeled structures was measured using the same threshold and particle size range to distinguish from the background and other structures (eg, red blood cells). The total intensity of fluorescence from the immunolabeled nucleosome depositions in GBM was quantified from the mean intensity multiplied by the total labeled area (see Supplemental Data).

Statistical Analysis

Group results were statistically analyzed using IBM SPSS Statistics version 22 (IBM Corporation), in 1-way analysis of variance and post hoc Tukey's Honest Significant Difference tests. Values were determined as mean ± standard error of mean. The statistical significance levels were defined as $^{*}P < .01$ and $^{\#}P < .05$.

RESULTS

Parvovirus B19 Nonstructural Protein-Induced Apoptotic Bodies Elicit Double-Stranded Deoxyribonucleic Acid Antibodies in Nonautoimmune Mice

Presence of serum anti-dsDNA autoantibodies was tested at weeks 1, 4, and 8 postimmunization. Immunofluorescence patterns of *C luciliae* kinetoplast in the CLIFT assay demonstrated the presence or absence of anti-dsDNA antibodies as illustrated by representative fluorescence patterns of each treatment group (Figure 1A). Untreated and PBS-treated groups were negative; in contrast, positive fluorescence was evident in pristane and all ApoBods groups. Percentages of positive kinetoplasts were determined (Figure 1B); results of negative groups represented background reactivity. At every time point, a range of 50%–60% was observed in the pristane group, and the percentage was significantly greater than negative controls at week 1 and week 8 ($P = 0–.005$) and also greater than all ST ApoBods at week 8 ($P = .002–.02$). Percentages in B19V NS1 ApoBods groups at week 1 and week 4 tended to be elevated compared with untreated and PBS-treated groups. At week 8, percentages in the 100-μg B19V NS1 ApoBods-treated group were significantly greater than negatives ($P = 0–.001$) and all ST ApoBods-treated mice ($P = .005–.048$). Double-stranded DNA autoantibodies were also measured by ELISA (Figure 1C). The mean absorbance of negative controls and ST ApoBods-treated groups was comparable to assay background. The absorbance value in the pristane-treated group was significantly greater than negatives and ST ApoBods-treated groups at weeks 4 and 8 ($P < .01$). The absorbance in B19V NS1 ApoBods-treatment groups was also higher than negative controls and ST ApoBods groups. Particularly at week 8, anti-dsDNA antibody concentration increased in a B19V NS1 ApoBod dose-dependent manner. Furthermore, absorbance values at 100-μg B19V NS1 ApoBods were significantly greater than negatives and all ST ApoBods groups at weeks 1 and 8 ($P = 0–.016$).

The number of mice positive for dsDNA antibodies analyzed by both assays is summarized (Table 2). The correlated results of CLIFT and ELISA indicated that B19V NS1 ApoBods stimulated the production of autoantibodies in non-autoimmune mice. The antibody levels of pristane and 100-μg B19V NS1 ApoBods-treated groups were significantly greater than negatives and all ST ApoBods-treated groups. Therefore, week 8 was studied in subsequent experiments. Using the mean absorbance of untreated sera plus 3 SDs as a cut-off, with borderline values considered ≥90% but <100% of cut-off, serologic anti-dsDNA antibodies were determined at either positive or borderline level at week 8 for 100-μg (6 of 6 mice), 50-μg (5 of 6 mice), and 25-μg (4 of 6 mice) B19V NS1 ApoBods-treated groups. In addition, serum anti-eGFP antibodies were examined using ELISA, which demonstrated that all mice did not develop antibodies reactive towards eGFP (see Supplemental Figure 1).

Parvovirus B19-Induced Apoptotic Bodies Elicit Inflammation and Cellular Degeneration in Vital Organs

Brain, heart, liver, and kidney were examined by bright-field microscopy. Representative images are shown for pristane, B19V NS1 ApoBods (Figure 2), and ST ApoBods-treated groups (Supplemental Figure 2). Inflammation and cellular degeneration were scored by a modified scoring system (Table 1). In the brain, degenerative neurons were evident in pristane and all B19V NS1 ApoBods-treated groups (Figure 2A). However, demyelination was evident only in mice treated with 50- and 100-μg B19V NS1 ApoBods-treated groups, and it was prominent in the 100-μg B19V NS1 ApoBods-treated group. The histology of ST ApoBods sections (Figure 2A–D) were similar to the untreated and PBS groups (see Supplemental Figure 2), which showed regular architecture and cell distribution.

Semiquantification of histological severity scores supported imaging results; the scores of pristane and all B19V NS1 ApoBods groups were greater than negative controls and

Table 1. Histopathology Scoring System of the Brain, Heart, Liver, and Kidney[a]

Brain [Scores 0–8] (5 Images/Mouse)		Heart [Scores 0–13] (5 Images/Mouse)		Liver [Scores 0–12] (5 Images/Mouse)			Kidney [Scores 0–9] (30 Glomeruli/Group)		
Inflammation [0–4]	Neuronal Degeneration [0–4]	Inflammation [0–9]	Myocardial Degeneration [0–4]	Portal Inflammation [0–4]	Lobular Inflammation [0–4]	Hepatocyte Degeneration [0–4]	Inflammation [0–3]	Tubulointerstitial Lesions [0–3]	Glomerular Lesions [0–3]
Markers	Markers	Markers	Markers	Markers	Markers	Markers	Markers	Markers	Markers
- Inflammatory cells surrounding the degenerating neurons - Demyelination	- Cell shrinkage - Eosinophilic cytoplasm with shrunken pyknotic nucleus - Neuropil vacuolation	- Infiltration of inflammatory cells	- Myocyte vacuolation - Myocyte disarray - Interstitial cell proliferation	- Inflammatory cells infiltrated to hepatic portal	- Inflammatory cells infiltrated to hepatic periportal	- Hepatocyte shrinkage - Cell swelling (ballooning) - Cytoplasmic vacuolation	- Inflammatory cells infiltrated to perivascular - Arterial vasculitis	- Tubular basophilia-Tubular atrophy-Interstitial fibrosis	- Glomerular cell proliferation - Mesangial proliferation - Capillary thickening - Lobulation - Crescent formation - Hyalinosis - Granuloma
Scoring	Scoring	Scoring	Scoring	Scoring	Scoring	Scoring	Scoring	Scoring	Scoring
0 = None 1 = Minimal, scattered small foci (<25%) 2 = Mild, isolated foci (25%–50%) 3 = Moderate, multifocal (51%–75%) 4 = Marked, multiple foci, necrosis (>75%)	0 = None, 1 = Minimal, few scattered (<25%) 2 = Mild, isolated foci (25%–50%) 3 = Moderate, multifocal (51%–75%) 4 = Marked, coalescing groups of degenerative neurons (>75%)	Severity 0 = None 1 = Minimal, scattered inflammatory cells <10 cells 2 = Mild, larger foci of 10–100 cells 3 = Larger foci of >100 cells Extent 1 = Mild (<25%) 2 = Moderate (25%–75%) 3 = Severe (>75%) *Scores = severity x extent	0 = None 1 = Minimal (<25%) 2 = Mild (25%–50%) 3 = Moderate (51%–75%) 4 = Marked (>75%)	0 = None 1 = Minimal (<25%) 2 = Mild (25%–50%) 3 = Moderate (51%–75%) 4 = Marked (>75%)	0 = None 1 = Minimal (<25%) 2 = Mild (25%–50%) 3 = Moderate (51%–75%) 4 = Marked (>75%)	0 = None 1 = Minimal (<25%) 2 = Mild (25%–50%) 3 = Moderate (51%–75%) 4 = Marked (>75%)	0 = None 1 = Mild, <1/3 of section 2 = Moderate, 1/3–2/3 of section 3 = Marked, >2/3 of section	0 = None 1 = Mild, <1/3 of section 2 = Moderate, 1/3–2/3 of section 3 = Marked, >2/3 of section	0 = None 1 = Mild, glomerular cell proliferation 2 = Moderate, same as grade 1 with mesangial proliferation, lobulation, and hyaline droplet 3 = Marked, same as grade 2 with crescent and granuloma formation and/or hyalinosis

[a]The severity of inflammation and cellular degeneration in each organ were observed and scored according to specific markers [18–28].

Percentages in the table refer to the percentage of the whole section area.

A

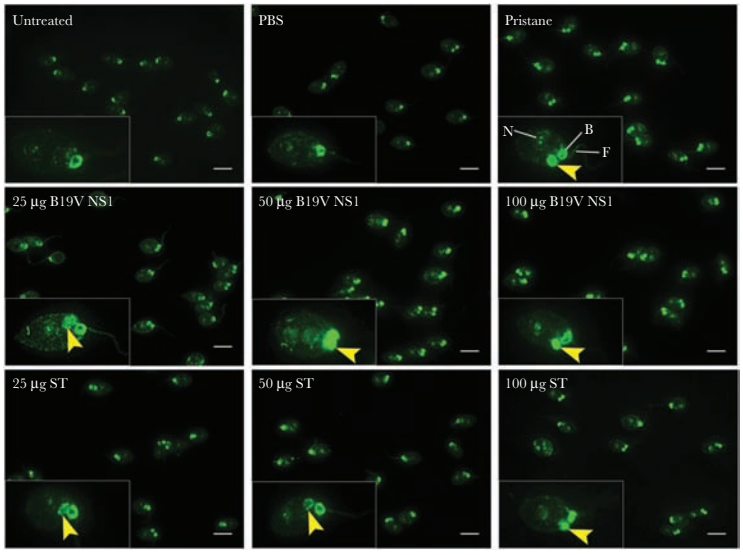

B

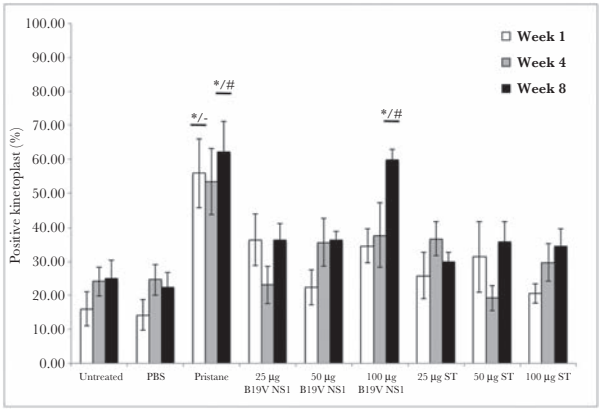

C

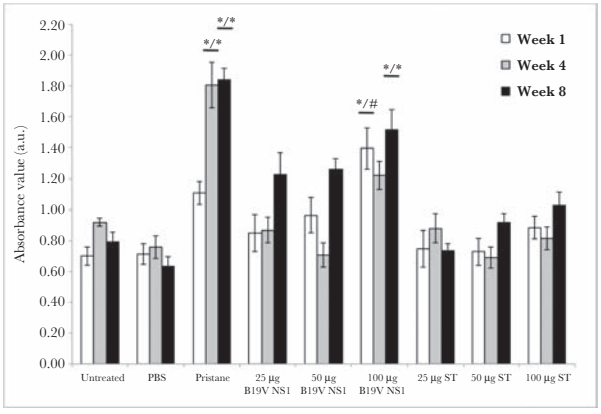

Figure 1. Parvovirus B19 (B19V) apoptotic bodies (ApoBods) are responsible for production of double-stranded deoxyribonucleic acid (dsDNA) autoantibody. (A) Fluorescence images of *Crithidia lucilae* immunofluorescent test (CLIFT) illustrate anti-dsDNA antibody levels in sera from differently treated mice at week 8 postimmunization. The presence of anti-dsDNA antibodies is determined by the positive green fluorescence of the kinetoplast (yellow arrowheads); an individual *C lucilae* cell representative of the positive population in each group is enlarged and displayed at the left lower corner of each panel. Kinetoplast is considered positive when its fluorescence intensity is the same or greater than the basal body (B), nucleus (N), or flagellum (F). Without fluorescence of kinetoplast, the cells are defined as negative. Bars, 10 µm. (B) Positive kinetoplasts stained with each mouse serum are counted out of 300 *C lucilae* cells. Percentages of positive kinetoplasts in each group ($n = 6$ mice/group) are calculated and presented as mean ± standard error of the mean (SEM). (C) Relative absorbance value of anti-dsDNA antibodies in each group assessed by the enzyme-linked immunosorbent assay and determined as mean ± SEM. Seropositive autoantibodies for each group are examined at week 1, 4, and 8 postimmunization, respectively. Results are compared with negative controls, untreated and phosphate-buffered saline (PBS)-treated groups, and all staurosporine (ST)-induced ApoBods groups, respectively. Significant difference considered as $^{\#}P < .05$ and $^{*}P < .01$, whereas – indicates nonsignificance.

Table 2. Autoantibodies to dsDNA Detected From Sera[a]

	Week 1				Week 4				Week 8			
	CLIFT		ELISA		CLIFT		ELISA		CLIFT		ELISA	
Treatments (6 Mice/Group)	Pos	Equi	Pos	Equi	Pos	Equi	Pos	Equi	Pos	Equi	Pos	Equi
Untreated	0	0	0	0	0	0	0	0	0	0	0	0
PBS	0	0	0	0	0	0	0	0	0	0	0	0
Pristane	4	0	4	0	4	1	6	0	3	1	6	0
25 μg B19V NS1	2	1	2	0	0	0	1	1	0	1	3	1
50 μg B19V NS1	0	1	1	1	1	1	0	0	0	0	2	3
100 μg B19V NS1	1	0	5	0	3	0	4	2	5	1	4	2
25 μg ST	2	0	1	0	1	1	1	1	0	0	0	0
50 μg ST	1	1	0	2	0	0	0	0	1	1	0	1
100 μg ST	0	0	0	0	1	0	1	0	0	1	1	0

Abbreviations: B19V, parvovirus B19; CLIFT, *Crithidia luciliae* immunofluorescence test; dsDNA, double-stranded deoxyribonucleic acid; ELISA, enzyme-linked immunosorbent assay; Equi, equivocal; NS1, nonstructural protein 1; PBS, phosphate-buffered saline; Pos, positive, ST, staurosporine.

[a]The CLIFT and ELISA assays were used to analyze autoantibodies against dsDNA in sera samples at week 1, 4, and 8 postimmunization. The number of positive samples per each group is indicated. The cut-off values at each time point for the CLIFT and ELISA assays are calculated by the mean percentage of the relative absorption unit of the untreated group plus 2 or 3 standard deviations of the mean of the untreated group, respectively. The cut-off values of CLIFT assay at week 1 = 40.49%, week 4 = 44.74%, and week 8 = 51.39%. The cut-off values of ELISA assay at week 1 = 1.133, week 4 = 1.110, and week 8 = 1.260. Values greater than cut-off are determined as Pos, whereas values higher than 90% but less than 100% of the cut-off are considered as Equi.

ST ApoBods groups ($P < .01$) (Figure 3A). In the heart, infiltration of immune cells was evident in pristine-treated mice and in mice treated with ApoBods induced by both B19V NS1 and ST. Inflammation in pristane-treated and B19V NS1 ApoBods-treated mouse hearts revealed severity (>50% of the whole area) higher than the ST ApoBods groups (<25% of the section area). Myocardial degeneration was marked in pristane and 100-μg B19V NS1 ApoBods groups ($P < .01$). Markers of myocardial degeneration were higher in the 100-μg B19V NS1 ApoBods-treated group than the 25- and 50-μg B19V NS1 ApoBods-treated groups. The semiquantitative severity scores of heart sections of pristane, as well as 50- and 100-μg B19V NS1 ApoBods groups, were significantly greater than negatives and ST ApoBods groups ($P < .01$) (Figure 3B). The severity score of the low concentration 25-μg B19V NS1 ApoBods was also significantly higher than negative controls ($P = .01$) and ST ApoBods-treated groups ($P = .05$).

In the liver, infiltrated immune cells were markedly evident in pristane-treated and all B19V NS1 ApoBods-treated groups. Degenerative signs and hepatocyte vacuolation were apparent only in the pristane group. However, histopathology severity scores of pristane and 100-μg B19V NS1 ApoBods groups were significantly higher than negatives and ST ApoBods groups ($P < .01$). Severity scores of 25- and 50-μg B19V NS1 ApoBods groups were significantly greater than negative ($P < .01$) and ST ApoBods groups ($P = -.05$). Finally, in the kidney, infiltrated immune cells and cellular degeneration were prominent in 50- and 100-μg B19V NS1 ApoBods similar to the pristane-treated group (>2/3 of the section) (Figure 2D). However, 25-μg B19V NS1 ApoBods also demonstrated these stigmata but at a slightly lower severity (1/3–2/3 of the section). Kidney sections of ST ApoBods-treated mice presented a few infiltrated immune cells without cellular degeneration; the architecture was similar to that of the negative controls (Supplemental Figure 2A-iv). Semiquantitative severity scores of pristane, as well as all 100-μg B19V NS1 ApoBods, were significantly greater than negatives and ST ApoBods groups ($P < .01$); those of 25- and 50-μg B19V NS1 ApoBods were higher than ST ApoBods ($P < .05$).

Glomerulonephritis and Systemic Lupus Erythematosus-Like Self-Antigen Deposition in Parvovirus B19 Nonstructural Protein Apoptotic Bodies-Treated Groups

Glomerulonephritis was determined by scoring the histopathological features (Table 1). Representative bright-field microscopy images are shown (Figure 4A and Supplemental Figure 2B-i). Typical glomerular structure was evident in the negative groups and all ST ApoBods-treated groups. Glomerulonephritis stigmata (glomerular cell proliferation, mesangial proliferation, and capillary thickening) were evident in pristane-treated and 50- and 100-μg B19V NS1 ApoBods-treated groups. Severity scores for inflammation, tubulointerstitial lesions, and glomerular lesions were at mild to moderate levels in pristane-treated and 100-μg B19V NS1 ApoBods-treated groups. Deposition of nucleosomal antigens in GBMs was investigated (Figure 4 and Supplemental Figure 2B). A nucleosomal antigen (dsDNA) was prominently deposited in the GBMs as expected. Staurosporine ApoBods groups had no deposited nucleosomal antigens in the glomeruli. The same sections were also stained with IgG to nucleosomal H1/H4/TBP; these nucleosomal antigens were detected at very low levels and not localized to the glomeruli (data not shown). The intensity of fluorescence from nucleosome depositions in each glomerulus was measured ($n = 30$ glomeruli/group), and that of deposited dsDNA was quantified,

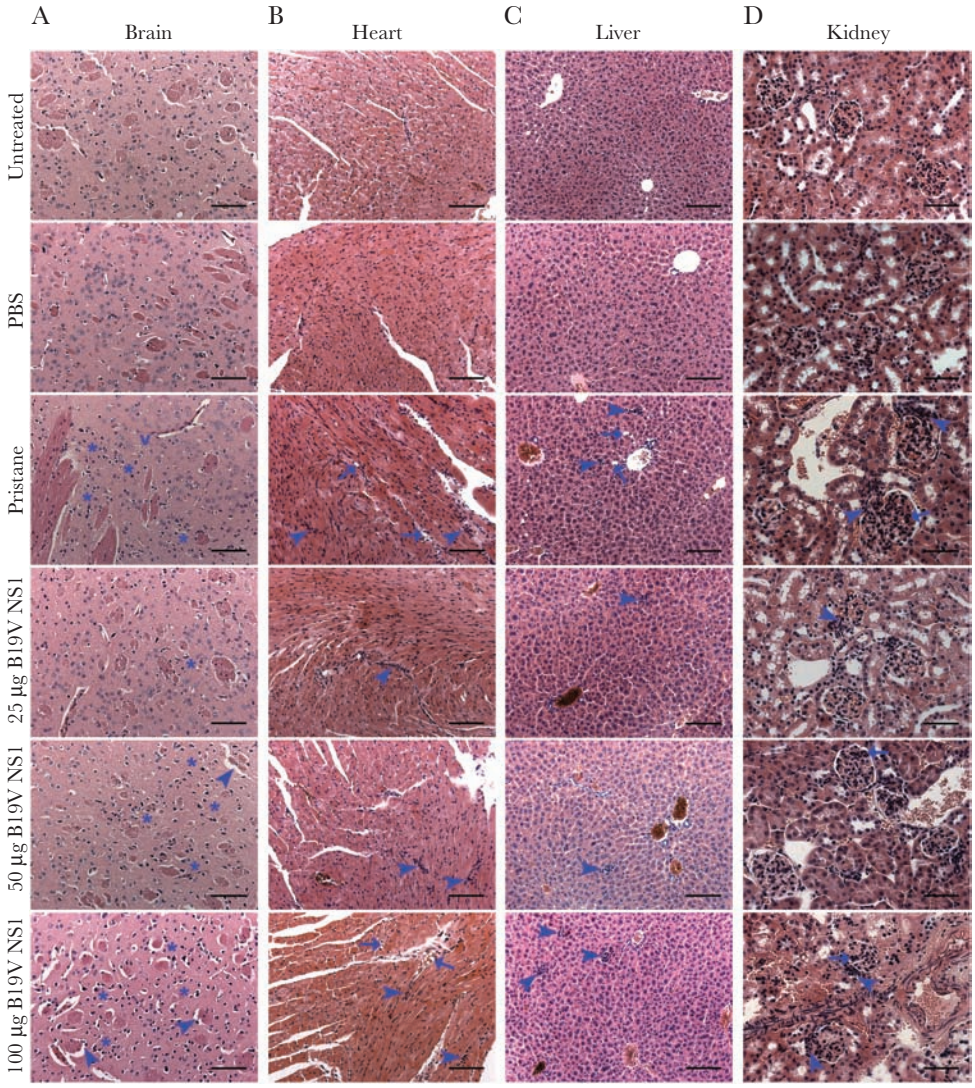

Figure 2. Apoptotic bodies stimulates inflammation and damage in major organs. Inflammation and cellular degeneration in mice organs are illustrated by the representative bright-field images of hematoxylin and eosin-stained sections of each treatment group. (A) Suspected demyelination (arrowheads), degenerating neurons with more than 6 cells surrounding the neuropil (asterisks), and neuropil vacuolation are indicated in the brain. (B and C) Infiltrated immune cells (arrowheads) and cellular vacuolation (arrows) are revealed in the heart and liver, respectively. (D) Infiltrated immune cells (arrowheads) and proliferated glomerular tissues (arrows) are observed in the kidney. Bars, 100 µm in A–C and 50 µm in D. B19V, parvovirus B19V; NS1, nonstructural protein 1; PBS, phosphate-buffered saline.

illustrated in the column scatters (Figure 5). The mean intensity of fluorescence of the pristane group was the highest, whereas all B19V NS1 ApoBods groups demonstrated approximately half of the pristane value. Pristane-treated groups, 50- and 100-µg B19V NS1 ApoBods-treated groups ($P < .01$), as well as 25-µg B19V NS1 ApoBods ($P < .05$) exhibited fluorescence intensity greater than negatives and ST ApoBods groups. Fluorescence intensity of H1/H4/TBP depositions was quantified and shown in Figure 5. Pristane-treated and 100-µg B19V NS1 ApoBods-treated groups were at comparable levels. The signal of pristane-treated and 100-µg B19V NS1 ApoBods-treated groups were significantly greater than negatives ($P = 0$) and ST ApoBods ($P = 0$–$.015$) groups.

DISCUSSION

Apoptotic Bodies Contribute to Autoimmunity

The onset of apoptosis at the late stages of viral infection is an important step in the life cycle of many viruses [29], including EBV [30] and B19V [9, 11, 31, 32], to spread progeny virions and evade host immune responses [29, 33]. The defective clearance of apoptotic cells and bodies may occur in viral infections because of increased apoptosis and decreased or absent phagocytic activities [34]. Defective clearance of apoptotic cells and bodies are factors that are thought to contribute to autoimmune disease [33–35]. In our study, SLE-like autoimmunity developed in non-autoimmune mice immunized with viral-induced ApoBods. Expression of autoantibodies against dsDNA as well

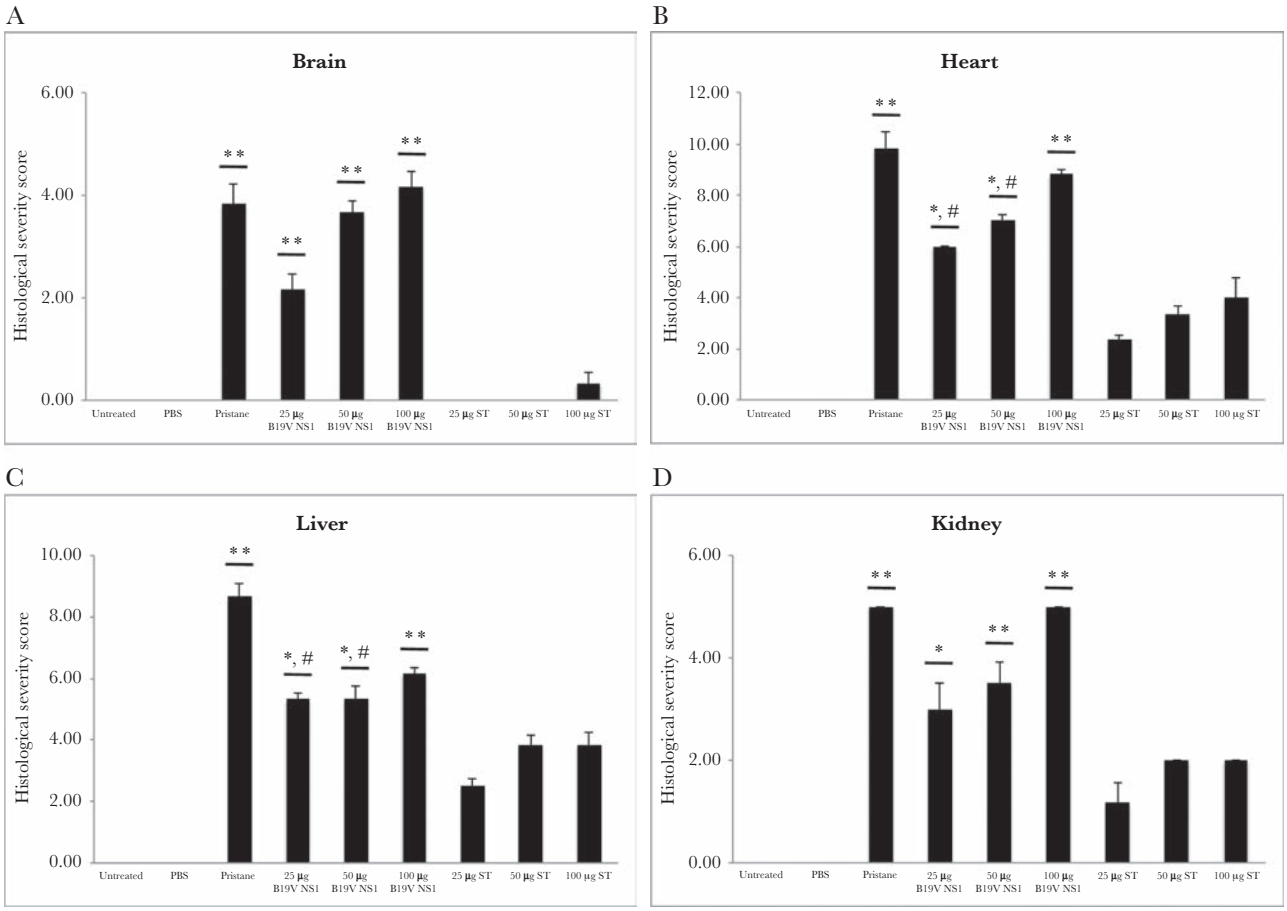

Figure 3. Significant histopathological destruction in major organs triggered by parvovirus B19 (B19V) apoptotic bodies (ApoBods). Histopathological severity of organs, including (A) brain, (B) heart, (C) liver, and (D) kidney were examined in every mouse. The severity scores are graded according to the histological features of inflammation and cellular degeneration. A severity score for each group ($n = 6$ mice/group) is determined as mean ± standard error of the mean. Results are compared with the negative controls, untreated and phosphate-buffered saline (PBS)-treated groups, and all staurosporine (ST)-induced ApoBods groups, respectively. Significant difference determined as $^{\#}P < .05$ and $^{*}P < .01$, whereas, – refers to nonsignificance.

as inflammation and damage in major organs were demonstrated (Figures 2 and 3). The site-specific organ inflammation we observed is consistent with a pathogenic role for ApoBods in autoimmunity [36]. The development of autoimmunity in animals immunized with apoptotic cells has been investigated, and those studies observed the production of self-reactive autoantibodies, eg, antinuclear antibody and anti-dsDNA antibody, but without development of histopathology [37, 38]. However, our study is the first to demonstrate the pathogenesis of autoimmunity by immunizing with virally induced ApoBods in vivo. In this instance, the ApoBods contained self-DNA covalently modified by B19V NS1 [9, 12]. Histological markers (Figure 4) and nucleosome deposition (Figure 5) in the glomeruli demonstrated the ability of virally induced ApoBods to induce GN. Renal injury may result from deposition of high concentrations of circulating antigen-antibody complexes [39]. Deposition of nucleosomes or chromatin fragments are likely the binding targets of autoantibodies that leads to lupus nephritis [40, 41]. These depositions, particularly dsDNA and anti-dsDNA antibody complexes, are essential markers of GN in SLE [42]. The deposition of dsDNA and anti-dsDNA antibodies complexes has been observed in both murine SLE models and human SLE [43]. In general, GN progresses after impaired clearance of apoptotic cells has occurred [44]. In addition, the development of GN has commonly developed in persistent viral infections, including EBV and B19V [4, 10].

Although viral infection has been proposed to play a role in the prototype autoimmune disease, SLE, the mechanism of the initial immunological insult remains unclear. It is paradoxical that anti-dsDNA is the hallmark pathogenic biomarker of SLE given that purified DNA is a poor experimental immunogen. We previously demonstrated that B19V infection of cells nonpermissive for virion production, eg, hepatocytes, express B19V nonstructural protein helicase, NS1, with minimal to no production of capsid protein [32]. The expression of NS1 induces apoptosis via the caspase 9 intrinsic pathway. Caspase 9 is activated as a consequence of NS1-mediated damage to host cell DNA [9, 11, 45, 46]. NS1 activates poly (ADP

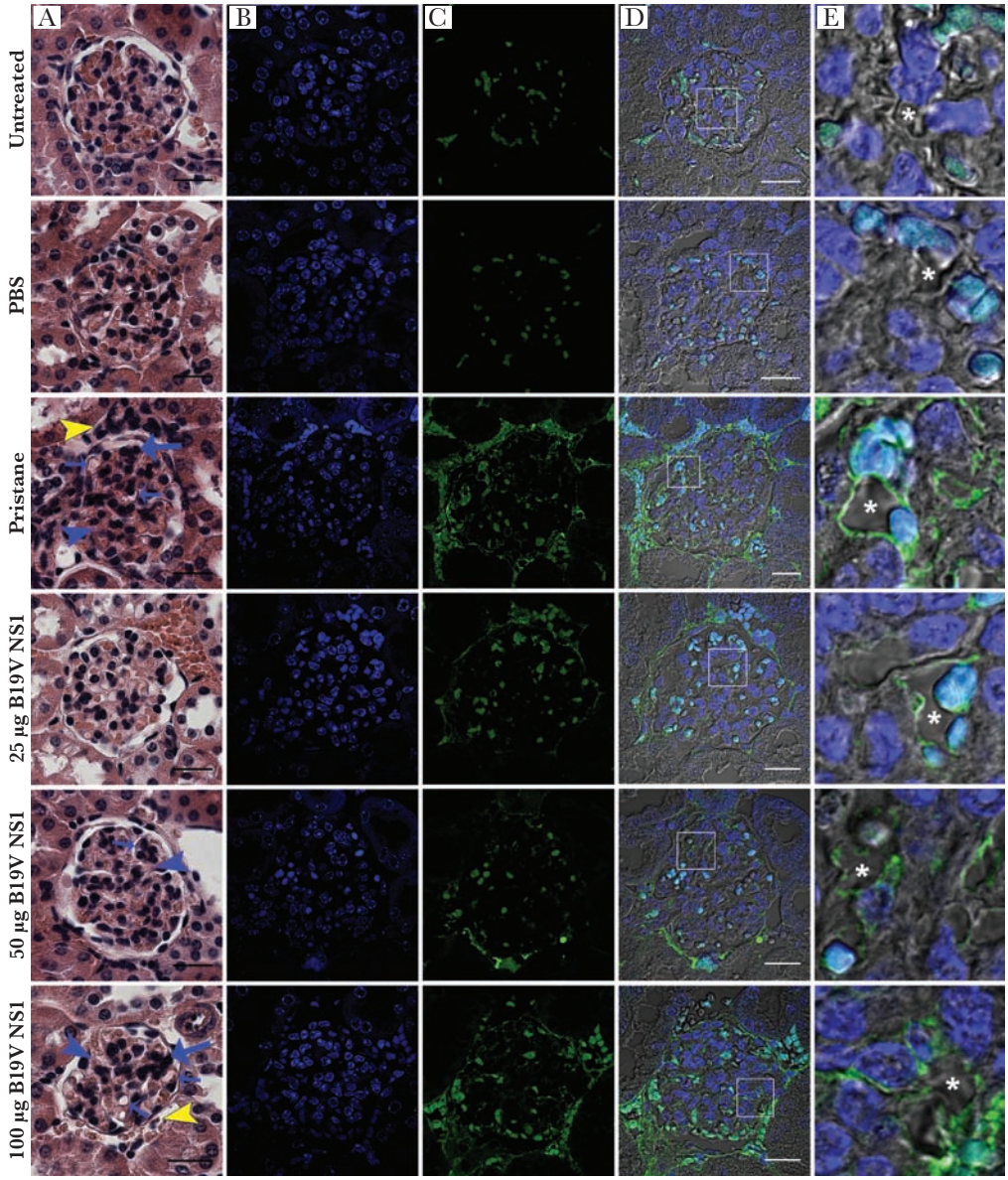

Figure 4. Parvovirus B19 (B19V) apoptotic bodies (ApoBods) induced glomerulonephritis (GN). (A) Bright-field microscopy images of hematoxylin and eosin-stained sections demonstrate histological alterations in a representative glomerulus of each group of controls and B19V nonstructural protein 1 (NS1)-induced ApoBods-treated groups. Histological features of GN, including infiltrated inflammatory cells (yellow arrowheads), glomerular cell proliferation (long blue arrows), mesangial proliferation (blue arrowheads), and glomerular capillary thickening (short blue arrows), were observed. Bars, 20 μm. Fluorescence images illustrate immunolabeled (B) cellular deoxyribonucleic acid (DNA) (4′,6-diamidino-2-phenylindole, blue) and (C) double-stranded (ds)DNA deposition in glomerular tissues (green). (D) Merge of B and C with differential interference contrast images demonstrate the morphology and location of deposited dsDNA self-antigen in the glomerulus. (E) Higher magnification of the area in white boxes in D indicate green signal of deposited dsDNA in glomerular basement membrane surrounding the glomerular capillary (asterisks). Turquoise represents the red blood cells. Bars, 20 μm. PBS, phosphate-buffered saline.

ribose) polymerase (PARP) as a response to NS1 single-strand nicking of host cell dsDNA. More central to development of autoimmunity, NS1 covalently links to host cell dsDNA to form bulky adducts. NS1 bulky adducts induce activation of ATM (ataxia-telangiectasia mutated)/ATR (ATM- and Rad3-Related) DNA repair pathways [9]. Both PARP and ATM/ATR repair pathways are energy depleting; extensive DNA damage and repair response depletes energy stores and presumably induces mitochondrial instability leading to caspase 9 activation [9]. We also previously demonstrated that NS1-modified self-DNA is incorporated into ApoBods along with DNA binding proteins and that these ApoBods are ingested by antigen-presenting cells (APCs) [12]. We hypothesized that APCs can process NS1 protein and present NS1 peptides to NS1-specific T lymphocytes [9]. Anergized dsDNA-specific B lymphocytes can internalize, via their anti-dsDNA B cell receptor, NS1 covalently linked to nucleosomal DNA. The B lymphocyte in turn can process and present NS1 peptides via major histocompatibility complex

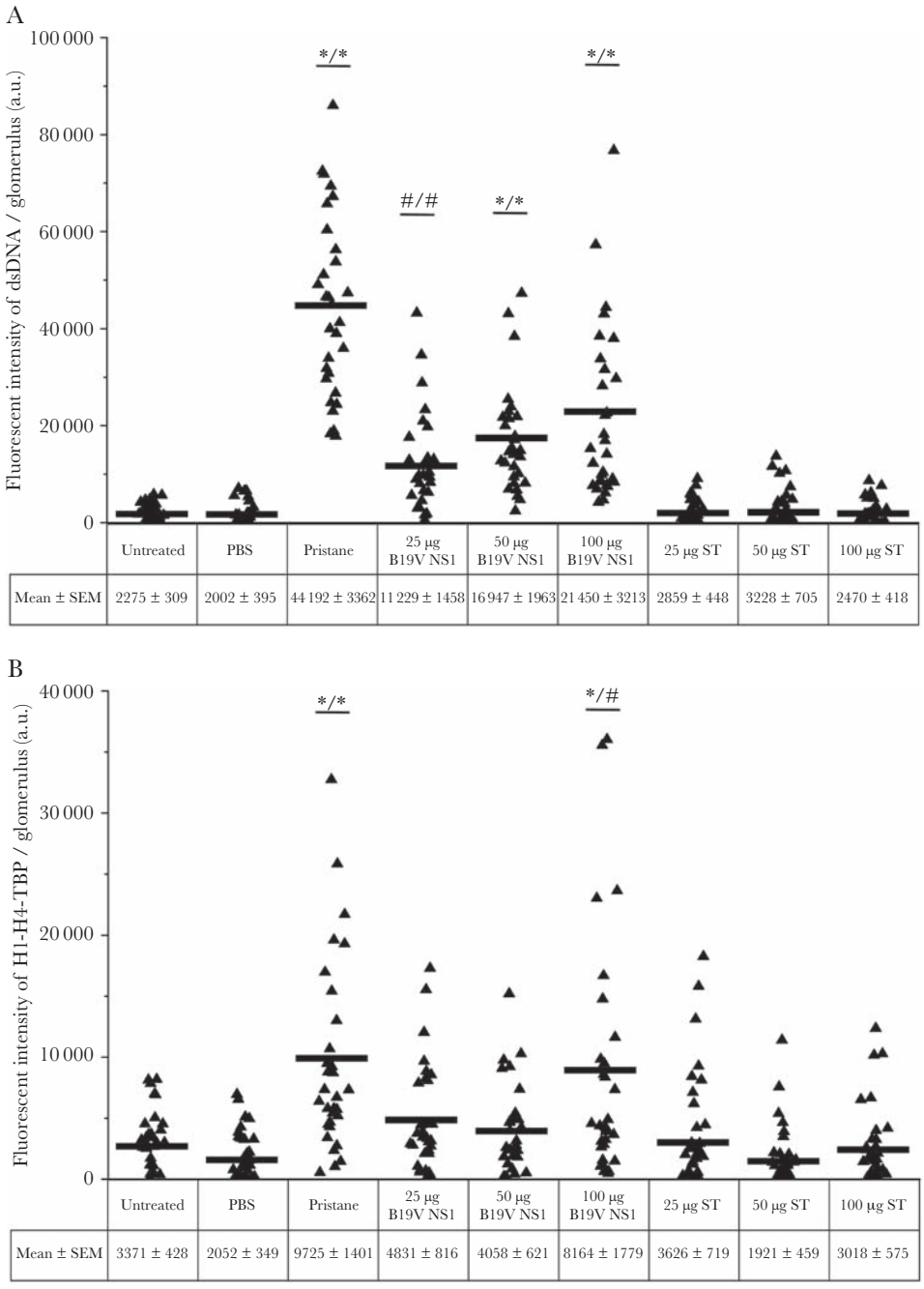

	Untreated	PBS	Pristane	25 μg B19V NS1	50 μg B19V NS1	100 μg B19V NS1	25 μg ST	50 μg ST	100 μg ST
Mean ± SEM	2275 ± 309	2002 ± 395	44 192 ± 3362	11 229 ± 1458	16 947 ± 1963	21 450 ± 3213	2859 ± 448	3228 ± 705	2470 ± 418

	Untreated	PBS	Pristane	25 μg B19V NS1	50 μg B19V NS1	100 μg B19V NS1	25 μg ST	50 μg ST	100 μg ST
Mean ± SEM	3371 ± 428	2052 ± 349	9725 ± 1401	4831 ± 816	4058 ± 621	8164 ± 1779	3626 ± 719	1921 ± 459	3018 ± 575

Figure 5. Deposition of self-antigens is detected in viral-induced glomerulonephritis. Nucleosomes deposition in glomeruli of each group was quantified from confocal microscopy images. Deposition of (A) double-stranded deoxyribonucleic acid (dsDNA) and (B) histone 1 (H1), H4, and TATA-binding protein (TBP) in the glomerular membrane were indicated by green and red fluorescence, respectively. A total of 30 glomeruli per group were analyzed. A triangle on a column scatter represents the fluorescence intensity of each glomerulus. Intensity from each group is determined as mean ± standard error of the mean (SEM). The mean intensity of each group is indicated in the scattered column. Results are compared with untreated and phosphate-buffered saline (PBS)-treated groups (left hand/ * or #), and then all staurosporine (ST)-induced apoptotic bodies (ApoBods) groups (/right hand * or #), respectively. Significant difference was defined as $^{\#}P < .05$ and $^{*}P < .01$.

to activated NS1-specific T lymphocytes, thereby receiving coactivation signals that break tolerance [9]. The current study supports our previous in vitro studies and provides proof of principle in an in vivo model.

The results indicate that the impact of NS1 on the induction of apoptosis and formation of ApoBods was key to breaking self-tolerance. Other members of this helicase family include tumor antigen of simian virus 40, E1 protein of human papillomavirus type 1a, E1 of bovine papillomavirus type 1, Rep40 of adenoassociated virus 2, and NS1 of porcine parvovirus [5, 7, 47]. These common viruses and their helicases share similar activities that cause DNA damage and apoptosis. Their helicases

and their interactions with viral dsDNA are essential to various steps in viral replication and the viral life cycle.

Our series of studies helps to explain observations by others that some cases of human SLE disease onset are preceded by several years by the appearance of antibodies to EBV nuclear antigen (EBNA) and that a shared epitope between EBNA and Sjögren syndrome A (SSA, or Ro) antigen leads to autoimmunity via epitope spreading [48, 49]. The B19V and EBV helicases are both members of the SF3 superfamily. We propose that the mechanism that breaks DNA tolerance and leads to autoimmunity that we demonstrated in our series of studies explains previous EBV observations in human SLE [47, 48]. It also explains why the presence of SSA antibodies are found in only a minority of SLE patients, in that SSA shows molecular mimicry with EBNA, but SF3 viral helicases other than EBNA, eg, B19V NS1, can induce antibodies to dsDNA. Because various helicases are encoded in bacteria, and viruses, inhibition of pathogen-specific helicase activity is a potential novel therapeutic target to prevent or control autoimmune disease [7].

CONCLUSIONS

In summary, the results in this study demonstrated how a common virus can break tolerance to self-DNA and promote pathogenesis of autoimmunity. We demonstrated that viruses are capable of triggering SLE-like disease by modifying self-DNA and inducing apoptosis and dsDNA autoantibodies, leading to pathology. These results encourage development of novel therapeutic strategies to prevent the progression of autoimmunity after viral infections.

Supplementary Data

Supplementary materials are available at *The Journal of Infectious Diseases* online. Consisting of data provided by the authors to benefit the reader, the posted materials are not copyedited and are the sole responsibility of the authors, so questions or comments should be addressed to the corresponding author.

Notes

Disclaimer. This work is unrelated to L. G.'s and S. J. N.'s commercial activities.

Financial support. This study was funded by The Schwartz Foundation (Mount Laurel, NJ).

Potential conflicts of interest. L. G. is chief executive officer of Te?ted Oy (Jyvaskyla, Finland). S. J. N. is employed by Quest Diagnostics Inc. (Secaucus, NJ) (salary, stock, stock options). All authors have submitted the ICMJE Form for Disclosure of Potential Conflicts of Interest. Conflicts that the editors consider relevant to the content of the manuscript have been disclosed.

References

1. Shapira Y, Agmon-Levin N, Shoenfeld Y. Defining and analyzing geoepidemiology and human autoimmunity. J Autoimmun **2010**; 34:J168–77.
2. Cohen BJ, Buckley MM. The prevalence of antibody to human parvovirus B19 in England and Wales. J Med Microbiol **1988**; 25:151–3.
3. Barzilai O, Sherer Y, Ram M, Izhaky D, Anaya JM, Shoenfeld Y. Epstein-Barr virus and cytomegalovirus in autoimmune diseases: are they truly notorious? A preliminary report. Ann N Y Acad Sci **2007**; 1108:567–77.
4. Posnett DN, Yarilin D. Amplification of autoimmune disease by infection. Arthritis Res Ther **2005**; 7:74–84.
5. James JA, Escalante CR, Yoon-Robarts M, Edwards TA, Linden RM, Aggarwal AK. Crystal structure of the SF3 helicase from adeno-associated virus type 2. Structure **2003**; 11:1025–35.
6. Kerr JR. The role of parvovirus B19 in the pathogenesis of autoimmunity and autoimmune disease. J Clin Pathol **2016**; 69:279–91.
7. Shadrick WR, Ndjomou J, Kolli R, Mukherjee S, Hanson AM, Frick DN. Discovering new medicines targeting helicases: challenges and recent progress. J Biomol Screen **2013**; 18:761–81.
8. Gorbalenya AE, Koonin EV, Wolf YI. A new superfamily of putative NTP-binding domains encoded by genomes of small DNA and RNA viruses. FEBS Lett **1990**; 262:145–8.
9. Poole BD, Kivovich V, Gilbert L, Naides SJ. Parvovirus B19 nonstructural protein-induced damage of cellular DNA and resultant apoptosis. Int J Med Sci **2011**; 8:88–96.
10. Tsay GJ, Zouali M. Unscrambling the role of human parvovirus B19 signaling in systemic autoimmunity. Biochem Pharmacol **2006**; 72:1453–9.
11. Kivovich V, Gilbert L, Vuento M, Naides SJ. The putative metal coordination motif in the endonuclease domain of human Parvovirus B19 NS1 is critical for NS1 induced S phase arrest and DNA damage. Int J Biol Sci **2012**; 8:79–92.
12. Thammasri K, Rauhamäki S, Wang L, et al. Human parvovirus B19 induced apoptotic bodies contain altered self-antigens that are phagocytosed by antigen presenting cells. PLoS One **2013**; 8:e67179.
13. Arbuckle MR, McClain MT, Rubertone MV, et al. Development of autoantibodies before the clinical onset of systemic lupus erythematosus. N Engl J Med **2003**; 349:1526–33.
14. Hahn BH. Antibodies to DNA. N Engl J Med **1998**; 338:1359–68.
15. Satoh M, Reeves WH. Induction of lupus-associated autoantibodies in BALB/c mice by intraperitoneal injection of pristane. J Exp Med **1994**; 180:2341–6.
16. Ruehl-Fehlert C, Kittel B, Morawietz G, et al. Revised guides for organ sampling and trimming in rats and mice–part 1. Exp Toxicol Pathol **2003**; 55:91–106.
17. Crowther JR. The ELISA Guidebook. Totowa, NJ: Humana Press; **2001**.
18. Fenyk-Melody JE, Garrison AE, Brunnert SR, et al. Experimental autoimmune encephalomyelitis is

exacerbated in mice lacking the NOS2 gene. J Immunol **1998**; 160:2940–6.
19. Kuhlmann T, Lassmann H, Brück W. Diagnosis of inflammatory demyelination in biopsy specimens: a practical approach. Acta Neuropathol **2008**; 115:275–87.
20. Garman RH. Histology of the central nervous system. Toxicol Pathol **2011**; 39:22–35.
21. McCarthy MK, Procario MC, Twisselmann N, et al. Proinflammatory effects of interferon gamma in mouse adenovirus 1 myocarditis. J Virol **2015**; 89:468–79.
22. Dunnick JK, Lieuallen W, Moyer C, Orzech D, Nyska A. Cardiac damage in rodents after exposure to bis(2-chloroethoxy)methane. Toxicol Pathol **2004**; 32:309–17.
23. Jokinen MP, Lieuallen WG, Boyle MC, Johnson CL, Malarkey DE, Nyska A. Morphologic aspects of rodent cardiotoxicity in a retrospective evaluation of National Toxicology Program studies. Toxicol Pathol **2011**; 39:850–60.
24. Brunt EM. Grading and staging the histopathological lesions of chronic hepatitis: the Knodell histology activity index and beyond. Hepatology **2000**; 31:241–6.
25. Thoolen B, Maronpot RR, Harada T, et al. Proliferative and nonproliferative lesions of the rat and mouse hepatobiliary system. Toxicol Pathol **2010**; 38:5S–81S.
26. Singh RR, Saxena V, Zang S, et al. Differential contribution of IL-4 and STAT6 vs STAT4 to the development of lupus nephritis. J Immunol **2003**; 170:4818–25.
27. Miyazaki T, Ono M, Qu WM, et al. Implication of allelic polymorphism of osteopontin in the development of lupus nephritis in MRL/lpr mice. Eur J Immunol **2005**; 35:1510–20.
28. Mina-Osorio P, LaStant J, Keirstead N, et al. Suppression of glomerulonephritis in lupus-prone NZB × NZW mice by RN486, a selective inhibitor of Bruton's tyrosine kinase. Arthritis Rheum **2013**; 65:2380–91.
29. Teodoro JG, Branton PE. Regulation of apoptosis by viral gene products. J Virol **1997**; 71:1739–46.
30. Larochelle B, Flamand L, Gourde P, Beauchamp D, Gosselin J. Epstein-Barr virus infects and induces apoptosis in human neutrophils. Blood **1998**; 92:291–9.
31. Hsu TC, Wu WJ, Chen MC, Tsay GJ. Human parvovirus B19 non-structural protein (NS1) induces apoptosis through mitochondria cell death pathway in COS-7 cells. Scand J Infect Dis **2004**; 36:570–7.
32. Poole BD, Karetnyi YV, Naides SJ. Parvovirus B19-induced apoptosis of hepatocytes. J Virol **2004**; 78:7775–83.
33. Gaipl US, Voll RE, Sheriff A, Franz S, Kalden JR, Herrmann M. Impaired clearance of dying cells in systemic lupus erythematosus. Autoimmun Rev **2005**; 4:189–94.
34. Muñoz LE, Janko C, Schulze C, et al. Autoimmunity and chronic inflammation - two clearance-related steps in the etiopathogenesis of SLE. Autoimmun Rev **2010**; 10:38–42.
35. Elliott MR, Ravichandran KS. Clearance of apoptotic cells: implications in health and disease. J Cell Biol **2010**; 189:1059–70.
36. Watson SC, Hughes F, Savill J. Apoptosis and glomerulonephritis. In: *Apoptosis and Its Relevance to Autoimmunity.* Vol. 9. New York: Karger, **2006**: pp 188–204.
37. Mevorach D, Zhou JL, Song X, Elkon KB. Systemic exposure to irradiated apoptotic cells induces autoantibody production. J Exp Med **1998**; 188:387–92.
38. Bondanza A, Zimmermann VS, Dell'Antonio G, et al. Cutting edge: dissociation between autoimmune response and clinical disease after vaccination with dendritic cells. J Immunol **2003**; 170:24–7.
39. Weening JJ, D'Agati VD, Schwartz MM, et al. The classification of glomerulonephritis in systemic lupus erythematosus revisited. J Am Soc Nephrol **2004**; 15:835–6.
40. Kalaaji M, Mortensen E, Jørgensen L, Olsen R, Rekvig OP. Nephritogenic lupus antibodies recognize glomerular basement membrane-associated chromatin fragments released from apoptotic intraglomerular cells. Am J Pathol **2006**; 168:1779–92.
41. Hedberg A, Mortensen ES, Rekvig OP. Chromatin as a target antigen in human and murine lupus nephritis. Arthritis Res Ther **2011**; 13:214.
42. Grootscholten C, van Bruggen MC, van der Pijl JW, et al. Deposition of nucleosomal antigens (histones and DNA) in the epidermal basement membrane in human lupus nephritis. Arthritis Rheum **2003**; 48:1355–62.
43. Berden JH, Licht R, van Bruggen MC, Tax WJ. Role of nucleosomes for induction and glomerular binding of autoantibodies in lupus nephritis. Curr Opin Nephrol Hypertens **1999**; 8:299–306.
44. Lleo A, Selmi C, Invernizzi P, Podda M, Gershwin ME. The consequences of apoptosis in autoimmunity. J Autoimmun **2008**; 31:257–62.
45. Poole BD, Zhou J, Grote A, Schiffenbauer A, Naides SJ. Apoptosis of liver-derived cells induced by parvovirus B19 nonstructural protein. J Virol **2006**; 80:4114–21.
46. Kivovich V, Gilbert L, Vuento M, Naides SJ. Parvovirus B19 genotype specific amino acid substitution in NS1 reduces the protein's cytotoxicity in culture. Int J Med Sci **2010**; 7:110–9.
47. Hickman AB, Dyda F. Binding and unwinding: SF3 viral helicases. Curr Opin Struct Biol **2005**; 15:77–85.
48. Harley JB, James JA. Epstein-Barr virus infection induces lupus autoimmunity. Bull NYU Hosp Jt Dis **2006**; 64:45–50.
49. Arbuckle MR, McClain MT, Rubertone MV, et al. Development of autoantibodies before the clinical onset of systemic lupus erythematosus. N Engl J Med **2003**; 349:1526–33.